

Guided modes in photonic structures with left-handed components

P Markoš

Faculty of Mathematics, Physics and Informatics, Comenius University in Bratislava
Mlynská dolina 2, 842 28 Bratislava, Slovakia

E-mail: `peter.markos@fmph.uniba.sk`

Abstract. The spectrum of guided modes of linear chain of dielectric and left-handed cylinders is analyzed. The structure of eigenfrequencies is much more richer if cylinders are made from the left-handed material with both permittivity and permeability negative. The number of guided modes is much larger, and their interaction with incident electromagnetic wave is much stronger. For some value of the wave vector, no guided modes were found. We discuss how these specific properties of guided modes correspond to folded bands, observed recently in photonic structures with left-handed components.

PACS numbers: 42.70.Qs

Keywords: photonic structures, Fano resonances, left-handed materials

Submitted to: *J. Phys. B: At. Mol. Phys.*

1. Introduction

Spatial periodicity of photonic structures composed from two dielectric materials is responsible for a broad variety of interesting physical phenomena. Band structure of frequency spectrum, appearance of gaps of forbidden frequencies [1, 2, 3], bound states [4], surface states [5] and guided modes in periodic structures [6, 7] represent only a few of them. Artificial metal – composite with negative effective permittivity can be constructed when one material is supplied by metal [8, 9, 10].

Discovery of left-handed materials [11, 12] with simultaneously negative permittivity and permeability, naturally addresses the question whether such materials could be used in the construction of new photonic structures and how negativity's of permittivity and permeability influence properties of resulting composite. Already in one dimensional systems, a new gap associated with zero mean value of refractive index was observed [13]. In two dimensional photonic crystals, the use of left-handed components led to the existence of folded bands with zero density of states for a certain interval of wave vectors [14, 15]. Numerical calculation of the transmission coefficients for photonic crystals with left-handed cylinders led to unexpected numerical instabilities when standard numerical methods were used [16]. Typical example of such instability is shown below in figure 8 which shows numerical data for transmission coefficient obtained by the transfer matrix algorithm for different spatial discretization give inconsistent results, which do not converge even in the limit of the most accurate accessible numerical approximation. Physically, such numerical instability indicates that the spatial distribution of electromagnetic field inside the photonic structure is strongly inhomogeneous [17].

In this paper we suggest that unusual properties of periodic photonic structures with left-handed components are due to excitation of broad spectra of guided modes which interact with incident electromagnetic wave. We show that indeed photonic structures with left-handed component support the excitation of a broad variety of spatially inhomogeneous guided modes which strongly influence the transmission of electromagnetic waves.

The paper is organized as follows: in Section 2 we describe the model and derive mathematical equations for guided modes in the most simple photonic structure: the linear chain of cylinders. Obtained system of linear equations is used in Section 3 to calculate of complete spectrum of guided modes both inside and outside the light cone. In Section 4 we use our numerical method for the calculation of the transmission through of plane electromagnetic wave through our structures. For dielectric cylinders, we proved that Fano resonance observed in the transmission spectra are due to the excitation of leaky guided modes [1, 6, 7]. Much stronger interaction of transmitted wave with guided modes is found in structures containing left-handed cylinders. Conclusion is given in Section 5.

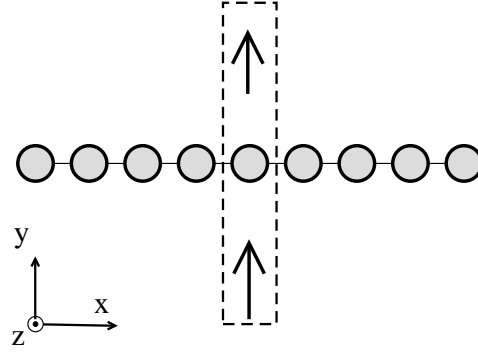


Figure 1. Structure consists from periodic linear chain of homogeneous cylinders of infinite length in the z direction. Cylinders have relative permittivity ε and permeability μ . We consider $\varepsilon = 12$ and $\mu = 1$ for the dielectric cylinder, and $\varepsilon = -12$ and $\mu = -1$ when cylinders are made from the left-handed material. The chain is located along the line $y = 0$. Central cylinder is located at $x, y = 0, 0$. The structure is periodic in the x direction with period a . The radius of cylinders is $R = 0.3a$. Electromagnetic wave impinges on the structure in y direction with polarization $E \parallel z$ or $H \parallel z$. Since the structure is periodic in the x direction, it is sufficient to consider only one unit cell.

2. The model

The structure of interest consists of an infinite periodic chain of cylinders embedded in the vacuum. (figure 1) Distance between cylinders, a , defines spatial periodicity of the structure along the x direction. Cylinders are infinite along the z direction, have radius $R = 0.3a$ and are made from homogeneous material with relative permittivity ε and permeability μ . We chose $\varepsilon = +12$, $\mu = +1$ for dielectric cylinders, and $\varepsilon = -12$, $\mu = -1$ for cylinders made from left-handed material.

We are interested in eigenstates propagating along the x direction with wave vector q and frequency ω . If (q, ω) lies inside the light cone (leaky modes with $q < \omega/c$), these states could couple to incident electromagnetic field.

2.1. Equations for guided modes

Consider first the E_z polarized electromagnetic wave. For the central cylinder, we express the electric intensity e_z and tangential component of the magnetic intensity h_t in terms of Bessel functions [18]. Inside the cylinder ($r \leq R$) we find

$$\begin{aligned} e_z^{\text{in}}(r, \varphi) &= \mathcal{J}_0 \alpha_0^+ + 2 \sum_{k>0} \alpha_k^+ \mathcal{J}_k \cos(k\varphi) + 2i \sum_{k>0} \alpha_k^- \mathcal{J}_k \sin(k\varphi) \\ -iZ h_t^{\text{in}}(r, \varphi) &= \mathcal{J}_0' \alpha_0^+ + 2 \sum_{k>0} \alpha_k^+ \mathcal{J}_k' \cos(k\varphi) + 2i \sum_{k>0} \alpha_k^- \mathcal{J}_k' \sin(k\varphi) \end{aligned} \quad (1)$$

In equation 1 we used

$$\mathcal{J}_k = J_k(2\pi n r / \lambda), \quad \mathcal{J}_k' = J_k'(2\pi n r / \lambda) \quad (2)$$

where J_k , J'_k are the Bessel function ($k = 0, 1, \dots$) and their derivatives, $\lambda = 2\pi c/\omega$ is the wavelength of electromagnetic field in vacuum, $n = \sqrt{\varepsilon\mu}$ is the index of refraction of the cylinder and $Z = Z_0\sqrt{\mu/\varepsilon}$ (c is the light velocity in vacuum and Z_0 is the vacuum impedance). Unknown parameters α^+ and α^- determines amplitudes of even ($\propto \cos k\varphi$) and odd ($\propto \sin k\varphi$) cylindrical waves, respectively.

The electric and magnetic fields outside the central cylinder consist from two contributions: the first one is the field scattered on the central cylinder,

$$\begin{aligned} e_z^0(r, \varphi) &= \mathcal{H}_0\beta_0^+ + 2\sum_{k>0}\beta_k^+\mathcal{H}_k\cos(k\varphi) + 2i\sum_{k>0}\beta_k^-\mathcal{H}_k\sin(k\varphi) \\ -iZ_0h_t^0(r, \varphi) &= \mathcal{H}'_0\beta_0^+ + 2\sum_{k>0}\beta_k^+\mathcal{H}'_k\cos(k\varphi) + 2i\sum_{k>0}\beta_k^-\mathcal{H}'_k\sin(k\varphi) \end{aligned} \quad (3)$$

($r \geq R$) with free parameters β^+ and β^- . Here,

$$\mathcal{H}_k = H_k(2\pi r/\lambda), \quad \mathcal{H}'_k = H'_k(2\pi r/\lambda). \quad (4)$$

and $H_k(z) = J_k(z) + iY_k(z)$ is the first Hankel function [18, 19].

The second contribution to the external fields is represented by fields scattered from all other cylinders. For the n th one ($n = \pm 1, \pm 2, \dots, N_s$) we express electric and magnetic intensity in coordinates associated with the center of the cylinder (figure 2)

$$\begin{aligned} e_z^n(\xi_n, \theta_n) &= H_0(w_n)\beta_{n0}^+ + 2\sum_{k>0}\beta_{nk}^+H_k(w_n)\cos(k\theta_n) \\ &\quad + 2i\sum_{k>0}\beta_{nk}^-H_k(w_n)\sin(k\theta_n) \\ -iZ_0h_{t_n}^n(\xi_n, \theta_n) &= H'_0(w_n)\beta_{n0}^+ + 2\sum_{k>0}\beta_{nk}^+H'_k(w_n)\cos(k\theta_n) \\ &\quad + 2i\sum_{k>0}\beta_{nk}^-H'_k(w_n)\sin(k\theta_n) \end{aligned} \quad (5)$$

$$\begin{aligned} Z_0h_{r_n}^n(\xi_n, \theta_n) &= H_0(w_n)\beta_{n0}^+ + 2\sum_{k>0}\beta_{nk}^+\frac{k}{w_n}H_k(w_n)\cos(k\theta_n) \\ &\quad + 2i\sum_{k>0}\beta_{nk}^-\frac{k}{w_n}H_k(w_n)\sin(k\theta_n) \end{aligned}$$

where we use

$$w_n = 2\pi\xi_n/\lambda \quad (6)$$

Thanks to the periodicity of the model, coefficients β_{nk}^\pm of the n th cylinder could be expressed in terms of coefficients β_k^\pm as

$$\beta_{nk}^\pm = e^{iqna}\beta_k^\pm \quad (7)$$

Coefficients α and β could be calculated from the requirement of the continuity of fields e_z and h_φ at the surface of the cylinder:

$$e_z^{\text{in}}(R^-, \varphi) = e_z^{\text{out}}(R^+, \varphi) = e_z^0(R^+) + \sum_{n \neq 0} e_z^n(\xi_n, \theta_n) \quad (8)$$

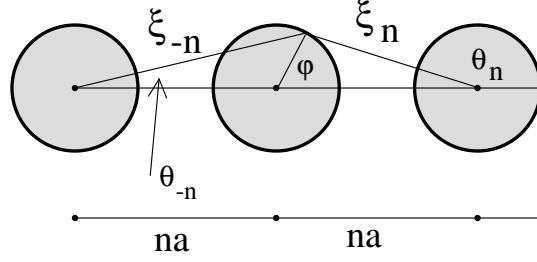


Figure 2. Parameters used in derivation of equation 5.

and

$$h_t^{\text{in}}(R^-) = h_t^{\text{out}} = h_t^0(R^+, \varphi) + \sum_{n \neq 0} [h_{t_n}^n(\xi_n, \theta_n) \cos \alpha_n - h_{r_n}^n(w_n, \theta_n) \sin \alpha_n] \quad (9)$$

where $\alpha_n = \theta_n - \varphi$.

Before solving this system of equations, we first transform all fields in equation 5 as a functions of R and φ . This can be done with the use of the Gegenbauer formula for cylindrical functions (figure 3)

$$H_m(w)e^{\pm im\chi} = \sum_{k=-\infty}^{+\infty} H_{m+k}(u)J_k(v)e^{\pm ik\alpha} \quad (10)$$

[19] and similar formula for the first derivative $H'_m(w)$:

$$H'_m(w)e^{\pm im\chi} = \sum_{k=-\infty}^{+\infty} H'_{m+k}(u)J_k(v)e^{\pm ik\alpha} \quad (11)$$

Inserting (11) into equations (5) we express, after some algebra, the fields at the outer boundary of the cylinder in the form

$$\begin{aligned} e_z^{\text{out}}(R^+, \varphi) &= \sum_{k,m=0}^N \mathbf{B}_{km} \beta_m^+ \cos k\varphi + \sum_{k,m=1}^N \mathbf{C}_{km} \beta_m^- \sin k\varphi \\ h_t^{\text{out}}(R^+, \varphi) &= \sum_{k,m=0}^N \mathbf{B}'_{km} \beta_m^+ \cos k\varphi + \sum_{k,m=1}^N \mathbf{C}'_{km} \beta_m^- \sin k\varphi \end{aligned} \quad (12)$$

Where we introduced N as the highest order Bessel function used in the expressions of the fields. Explicit form of matrices \mathbf{B} , \mathbf{B}' , \mathbf{C} and \mathbf{C}' is given in the Appendix A.

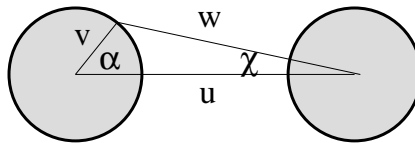


Figure 3. Parameters used in Gegenbauer's relation, equations 10 and 11

Incident electromagnetic field contributes to the rhs of equation 12. We express it in the cylindrical coordinates

$$\begin{aligned} e_z^i(r, \varphi) &= J_0(v) + \sum_{k>0}^N e_k^+ \cos(k\varphi) + i \sum_{k>0}^N e_k^- \sin(k\varphi) \\ -iZ_0 h_\varphi^i(r, \varphi) &= J_0'(v) + \sum_{k>0}^N h_k^+ \cos(k\varphi) + i \sum_{k>0}^N h_k^- \sin(k\varphi) \end{aligned} \quad (13)$$

Inserting fields (1) and (2) into equations 8 and 9 we obtain the set of linear equations for even modes:

$$\mathbf{A}_k \alpha_k^+ = \sum_m \mathbf{B}_{km} \beta_m^+ + e_k^+ \quad (14)$$

$$\zeta \mathbf{A}'_k \alpha_k^+ = \sum_m \mathbf{B}'_{km} \beta_m^+ + h_k^+$$

($k = 0, 1, \dots, N$) and similar equations for odd modes

$$\mathbf{A}_k \alpha_k^- = \sum_m \mathbf{C}_{km} \beta_m^- + e_k^- \quad (15)$$

$$\zeta \mathbf{A}'_k \alpha_k^- = \sum_m \mathbf{C}'_{km} \beta_m^- + h_k^-$$

($k = 1, 2, \dots, N$). Here, $\zeta = Z/Z_0$, $\mathbf{A}_k = \mathcal{J}_k(2 - \delta_{k0})$ and $\mathbf{A}'_k = \mathcal{J}'_k(2 - \delta_{k0})$ (equation 1).

In the next step, we remove α^+ from equations 14 and obtain the system of linear equations for parameters β^+ :

$$\sum_m \left[\mathbf{B}_{km} - \zeta \frac{\mathcal{J}_k}{\mathcal{J}'_k} \mathbf{B}'_{km} \right] \beta_m^+ = e_k^+ - \zeta \frac{\mathcal{J}_k}{\mathcal{J}'_k} h_k^+, \quad k = 0, 1, \dots, N \quad (16)$$

and equivalent equation for parameters β^- :

$$\sum_m \left[\mathbf{C}_{km} - \zeta \frac{\mathcal{J}_k}{\mathcal{J}'_k} \mathbf{C}'_{km} \right] \beta_m^- = e_k^- - \zeta \frac{\mathcal{J}_k}{\mathcal{J}'_k} h_k^-, \quad k = 1, 2, \dots, N \quad (17)$$

With known parameters β^\pm , we find α^\pm from equations 14 and 16.

In numerical analysis, we consider the number of cylinders $N_s = 100 - 4000$ and number of modes $N \leq 22$. We found that consideration of $N = 12$ modes is sufficient in most of analyzed problems.

2.2. Transmission coefficient

Transmission coefficient can be calculated as the ratio of the y -component of the Poynting vector $S_x(y_p)$, calculated for any $y_p > r$ to the incident Poynting vector, S_y^i

$$T = \frac{S_x(y_p)}{S_x^i} = \int_{-a/2}^{+a/2} dx e_z(x, y_p) h_x^*(x, y_p) / \int_{-a/2}^{+a/2} dx e_z^i(x, y_p) (h_x^i(x, y_p))^* \quad (18)$$

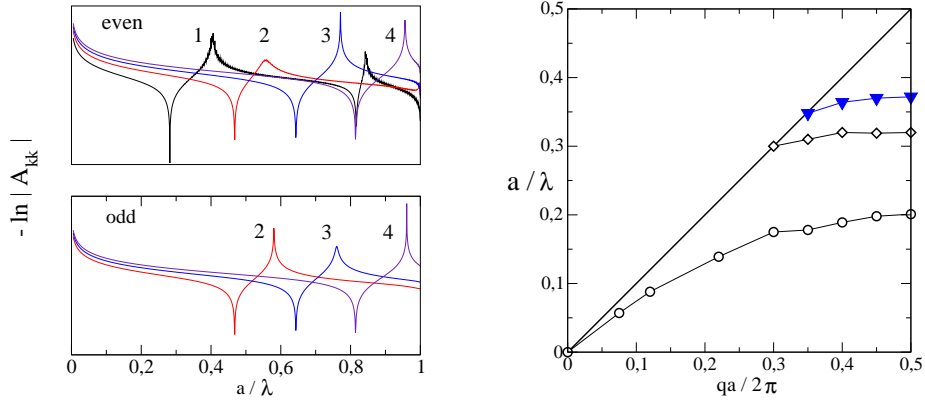


Figure 4. Guided modes of the chain of dielectric cylinders ($\varepsilon = 12$, $\mu = 1$). Left figure shows the frequency dependence of diagonal elements $\ln A_{kk}$ for $q = 0$ (equations 20 and 21). Four even modes and three odd modes can be identified. Right figures presents the spectrum of E_z polarized Open and closed symbols correspond to even modes ($n = 0$ and 1) and odd mode $n = 1$. Owing to the periodicity of the problem, it is sufficient to consider wave vectors $0 < q < \pi/a$ [1].

2.3. Polarization

The above analysis Can be repeated for the H_z polarized modes. It turns out that final equations (16) and 17) remain the same if we substitute

$$\zeta \rightarrow \frac{1}{\zeta} \quad (19)$$

and exchange of e_x and h_z in expression for the transmission coefficient (18).

3. Guided modes

Consider first equations 16 and 17 without incident electromagnetic wave. Then, the spectrum of guided modes can be found from the requirements of zero determinant

$$\det \left[\mathbf{B}_{km} - \zeta \frac{\mathcal{J}_k}{\mathcal{J}'_k} \mathbf{B}'_{km} \right] = 0 \quad (20)$$

and

$$\det \left[\mathbf{C}_{km} - \zeta \frac{\mathcal{J}_k}{\mathcal{J}'_k} \mathbf{C}'_{km} \right] = 0 \quad (21)$$

for even and odd modes, respectively.

With the use of Gauss-Jordan elimination method [20], we transform matrices in equations (20) and (21) to diagonal form and plot the frequency dependence of inverse of obtained diagonal elements A_{kk} . This enables us not only to find the eigenfrequency of guided modes and their lifetime [21], but also identify their symmetry. As an example, we show in the left figure 4 resonances of leaky guided modes with zero wave vector $q = 0$.

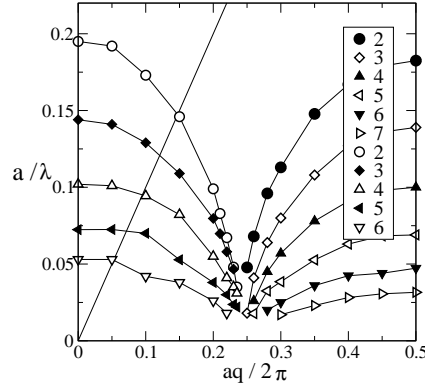


Figure 5. Spectrum of guided modes of the chain of cylinders made from the left-handed material ($\varepsilon = -12$, $\mu = -1$) cylinders. There are no modes around $q_c \approx 0.24 \times 2\pi/a$. Open and closed symbols correspond to even and odd modes, respectively. Note that guided modes changes symmetry when q crosses q_c .

Right figure 4 presents eigenfrequencies of guided modes as a function of wave vector q identified from the position of resonances in corresponding diagonal elements. We found two even modes with $k = 0$ and 1 and one odd mode $k = 1$, which agree with our expectation [1].

The spectrum of guided modes for left-handed cylinders is more complicated and consists of series of even and odd modes. In contrast to dielectric cylinders, the eigenfrequencies of guided modes decreases when mode index k increases. The number of modes depends on the model parameters and increases when absolute value of the refractive index increases.

Another unexpected property of guided modes is the existence of "critical value" of the wave vector q_c ($q_c \approx 0.247 \times 2\pi/a$ in our model) for which no guided mode exists (figure 5). Preliminary analysis of other left-handed structures with $\mu = -1$ (data not shown) indicates that q_c depends neither on (negative) permittivity nor on the radius of cylinder.

4. Interaction of external field with guided modes

We solve equations 16 and 17 and calculate transmission coefficient for incident plane wave with wavelength λ propagating along the y direction. First, we express the coefficients E_k^\pm and h_k^\pm

$$\begin{aligned} e_k^+ &= h_k^+ = J_k(v)(1 + (-1)^k)/(1 + \delta_{k0}) & k = 0, 1, \dots \\ e_k^- &= h_k^- = J_k(v)(1 - (-1)^k), & k = 1, 2, \dots \end{aligned} \quad (22)$$

($v = 2\pi R/\lambda$). From known coefficients β^+ and β^- we find spatial distribution of fields and calculate transmission coefficient given by equation 18.

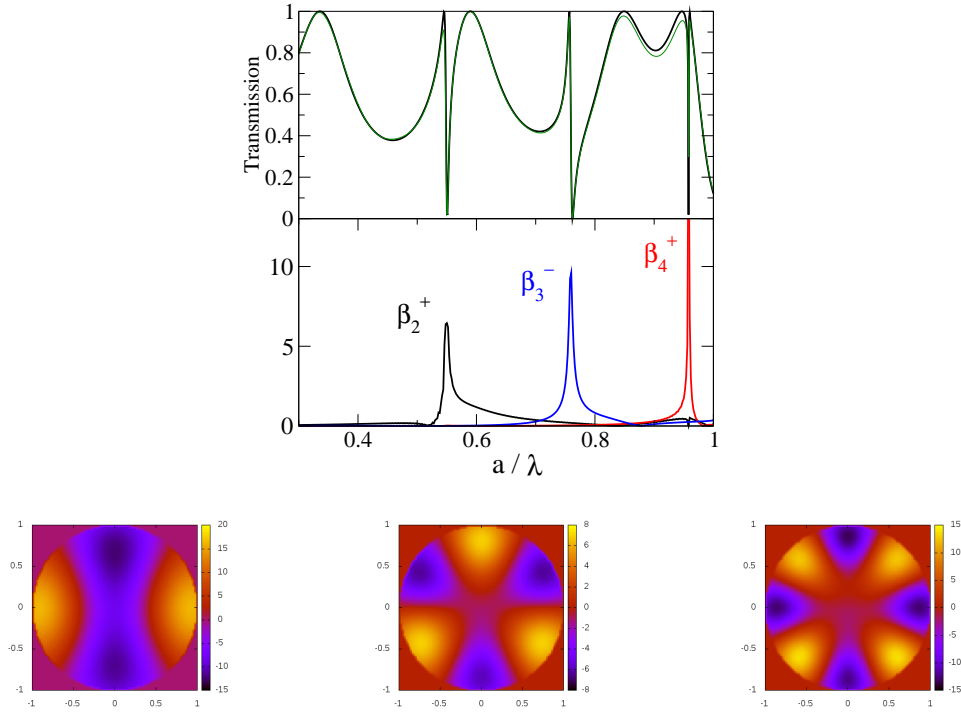


Figure 6. Transmission of the E_z polarized plane wave propagating through an infinite 1D chain of dielectric cylinders. Top panel displays the transmission coefficient as a function of a/λ , calculated by the transfer matrix method and by the formula (18). Three Fano resonances correspond to maxims of coefficients β shown in middle panel. Real part of the intensity of electric field inside the cylinder for three resonance frequencies, $a/\lambda = 0.549, 0.759$ and 0.958 is shown in the bottom panel.

4.1. Dielectric cylinders

Figure 6 shows the transmission coefficient for the E_z polarized plane electromagnetic wave as a function of wavelength. Obtained results agree very well with numerical data calculated by the transfer matrix method [23, 24]. Typical Fano resonances in the transmission spectra [6, 7] are clearly visible and could be associated with excitation of corresponding guided modes [22] in cylinder chain. Owing to the symmetry of the incident wave which does not depend on x , only modes symmetric with respect to $x \rightarrow -x$ could be excited. Two even modes with $k = 2$ and $k = 4$ and one odd mode ($k = 3$) have been excited. Bottom panels show the real part of electric field inside the cylinder and confirm predicted symmetry of excited states.

Similar results have been obtained also for the H_z polarized incident wave shown in figure 7. In this case, two resonances of $k = 0$ mode are clearly visible. The lower one, together with the first odd resonance, deform strongly the transmission spectrum. Three resonances observed at higher frequencies could be easily detected both from the transmission spectra and from the frequency dependence of parameters β .

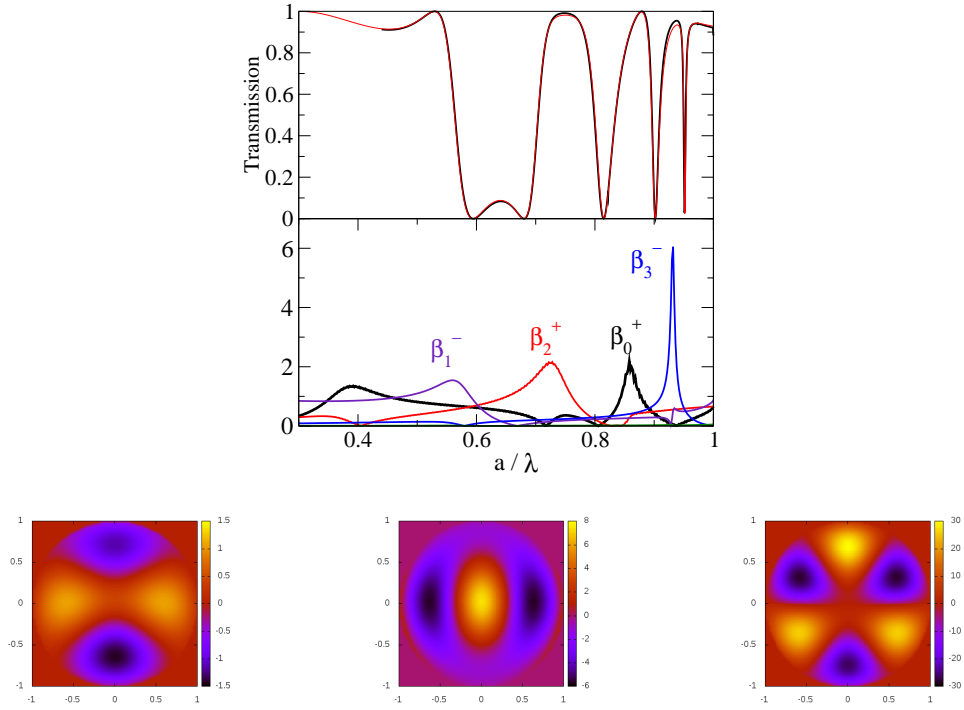


Figure 7. Transmission of the H_z polarized plane wave propagating through an infinite chain of dielectric cylinders. Top panel displays the transmission coefficient as a function of a/λ , calculated by the transfer matrix method and by the formula equation 18. Fano resonances correspond to maxims of coefficients β shown in middle panel. Real part of the intensity of magnetic field inside the cylinder for three resonance frequencies, $a/\lambda = 0.729, 0.865$ and 0.931 is shown in the bottom panel.

4.2. Left-handed cylinders

The same analysis of the transmission spectra of cylinders made from the left-handed medium ($\varepsilon = -12$, $\mu = -1$) is more difficult, since standard numerical techniques (transfer matrix method, RCWA) seem not to be suitable for the calculation of the transmission coefficient. As shown in the left panel of figure 8, results obtained by the transfer matrix method with three discretization of the unit cell provide us with completely different transmission coefficients. Such failure, obtained also when the transmission was calculated by the RCWA method indicates that the eigenstates of the electromagnetic field inside the structure are strongly inhomogeneous. Consequently, excited guided modes cannot be expanded in a finite series in the basis of eigenfrequencies, used in the transfer matrix method.

The assumption of strong spatial inhomogeneity is confirmed by frequency dependence of coefficients β shown in middle panel of figure 8. Incident electromagnetic wave excites in the left-handed chain a series of guided modes. The resonant frequencies of these modes lie very close to each other (in fact, since the resonances have a finite width, they overlap). Also, absolute values of coefficients β are in order of magnitude

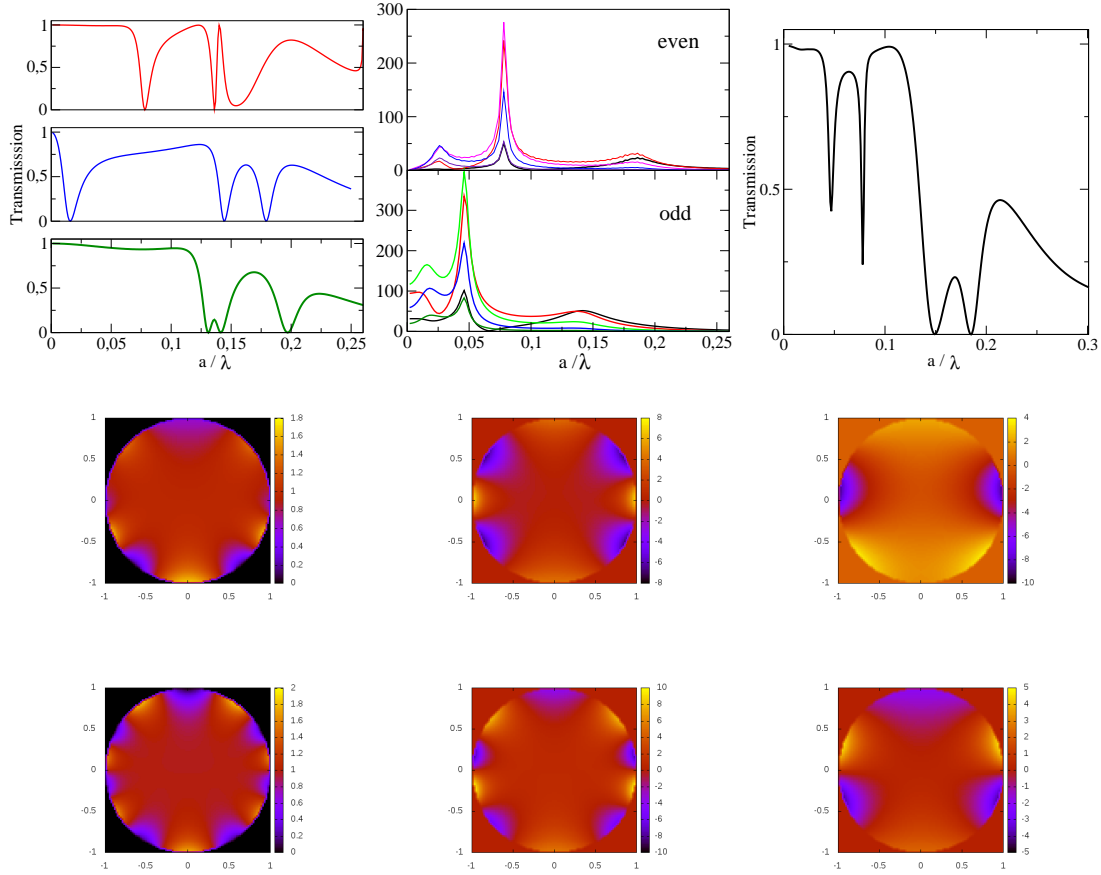


Figure 8. Left: transmission of the E_z polarized electromagnetic wave through the linear chain of left-handed cylinders calculated by the transfer-matrix method with three different space discretization (120, 240 and 360 mesh points per unit cell). Middle: spectrum of coefficients β . Note the scale of the vertical axis. Right panel shows the transmission coefficient calculated by the present method (equation 18). Bottom panel shows real part of the intensity of electric field inside the left-handed cylinder for frequencies associated with resonances of even modes ($a/\lambda = 0.027, 0.078$ and 0.184), and odd modes ($0.016, 0.047$ and 0.140).

larger than in the case of dielectric cylinder.

Right panel of figure 8 shows the transmission coefficient obtained by equation (18). Two minims in the transmission coefficient coincide with eigenfrequencies of excitation of guided modes. The spatial distribution of electric field shown in the bottom panel confirm that many resonances are excited simultaneously – in contrast to dielectric structure, we cannot easily identify the order of excited modes.

The above mentioned problem of numerical instability is not actual when transmission of the H_z polarized wave is calculated (figure 9). Now, numerical data obtained by the transfer matrix method agree perfectly with those found by the present method (left panel). As shown in the right panel, resonances of guided modes are very weak and broad, so that they have negligible influence on the transmission coefficient.

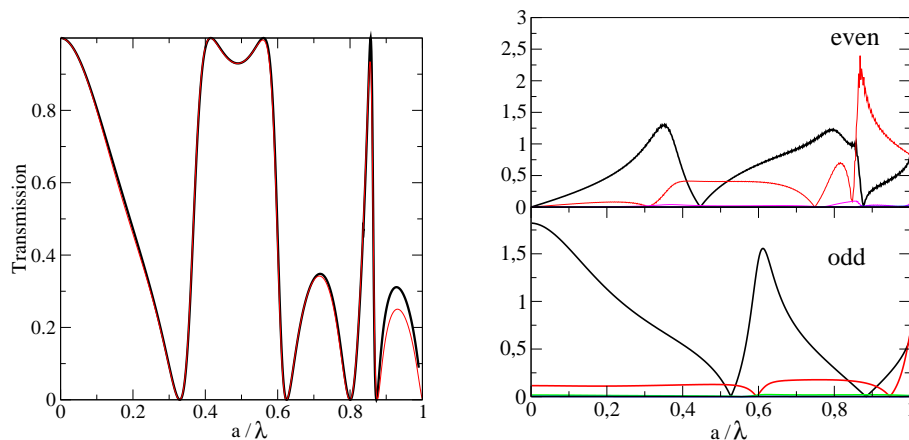


Figure 9. Left: Transmission of H_z -polarized plane wave through the chain of left-handed cylinders calculated by the transfer matrix method and from equation 18. Similarly to the case of dielectric cylinders, two numerical methods give identical result, because Fano resonances (shown in the right panel) are much weaker than in the case of E_z polarized wave (Fig. 8).

5. Conclusion

We presented physical and numerical analysis of the guided modes of linear chain of cylinders, made either from the dielectric or from the left-handed material. Comparison of these two structures shows new phenomena could be observed when permittivity and permeability possess negative values. We proved that the transmission of electromagnetic waves through the photonic structure with left-handed components is strongly influenced by guided modes excited in the structure.

The spectrum of guided modes contains much more branches. In contrast to dielectric structure, the eigenfrequency of these modes decreases when mode index k increases. Also, there are no guided modes for the wave vector close to some critical value q_c . We suppose that this absence of guided modes corresponds to the folding of frequency bands observed recently [15, 14].

Very rich spectrum of guided modes is responsible for numerical instabilities when the transmission coefficients is calculated by standard methods. Since eigenmodes of the left-handed structure strongly differs from plane waves, any numerical algorithm, based on the expansion of the fields into the plane waves (transfer matrix or RCWA) fails to recover true transmission coefficient.

6. Appendix A

For $k, m = 1, 2, \dots, N_B$, $J_k \equiv J_k(2\pi R/\lambda)$ and \mathcal{H}_k given by equation 4 we obtain the $N + 1 \times N + 1$ matrix \mathbf{B}

$$\begin{aligned} B_{00} &= \mathcal{H}_0 + \sum_{n=1}^{N_s} 2 \cos q H_0(un) J_0 \\ B_{0m} &= \sum_{n=1}^{N_s} H_m(un) J_0 \times [(-1)^m e^{iqan} + e^{-iqan}] \\ B_{k0} &= \sum_{n=1}^{N_s} H_k(un) J_k \times 2[e^{iqan} + (-1)^k e^{-iqan}] \end{aligned} \quad (23)$$

$$B_{km} = 2\mathcal{H}_k \delta_{km} + \sum_{n=1}^{N_s} [e^{iqan}(-1)^{m-k} + e^{-iqan}][H_{m-k}(un) + (-1)^k H_{m+k}(un)] J_k$$

and the $N \times N$ matrix \mathbf{C} :

$$\begin{aligned} C_{km} &= 2\mathcal{H}_k \delta_{km} + \sum_{n=1}^{N_s} [e^{iqan}(-1)^{m-k} + e^{-iqan}] \\ &\quad \times [\mathcal{H}_{m-k}(un) - (-1)^k \mathcal{H}_{m+k}(un)] J_k \end{aligned} \quad (24)$$

Matrices \mathbf{B}' and \mathbf{C}' could be obtained from \mathbf{B} and \mathbf{C} , respectively, by substitutions

$$J_k \rightarrow J'_k, \quad \mathcal{H}_k \rightarrow \mathcal{H}'_k \quad (25)$$

Acknowledgment

This work was supported by the Slovak Research and Development Agency under the contract No. APVV-0108-11 and by the Agency VEGA under the contract No. 1/0372/13.

References

- [1] Joannopoulos J D, Johnson S G Winn J N and Meade R G 2008 *Photonic Crystals: Molding the Flow of Light* 2nd edition. (Princeton: Princeton University Press)
- [2] Sakoda K 2005 *Optical Properties of Photonic Crystals* (Berlin, Heidelberg: Springer, 2005)
- [3] Soukoulis C M (editor) 2001 *Photonic Crystals and Light Localization in the 21st Century* (Dordrecht: Kluwer)
- [4] Robertson W M *et al.* 1992 *Phys. Rev. Lett.* **68** 2023
- [5] Robertson W M *et al.* 1993 *Optics Lett.* **18** (1993)
- [6] Fan S and Joannopoulos J D 2002 *Phys. Rev. B* **65** 235112
- [7] Fan S Suh W and Joannopoulos J D 2003 *J. Opt. Soc. Amm. A* **20** 569
- [8] Pendry J B *et al.* 1996 *Phys. Rev. Lett.* **76** 4773
- [9] Pokrovsky A L and Efros A L 2002 *Phys. Rev. Lett.* **89** 093901
- [10] Markoš P and Soukoulis C M 2003 *Optics Lett.* **28** 846
- [11] Pendry J B, Schurig D and Smith D R 2006 *Science* **312**, 1780
- [12] Engheta N and Ziolkowski R W (Editors) 2006 *Metamaterials: Physics and Engineering Explorations*. (New York: J. Wiley & Sons)

- [13] Li J *et al* 2003 *Phys. Rev. Lett.* **90** 083901
- [14] Hermann D *et al* 2008 *Phys. Rev. B* **77** 035112
- [15] Chen P Y *et al* 2011 *New J. Phys.* **13** 053007
- [16] Kajtár G 2014 *private communication*
- [17] Asatryan A A, Dossou K B and Botten L C 2008 *Australian Institute of Physics, 18th national Congress*
- [18] Stratton J A 1941 *Electromagnetic Theory* (New York: Mc Graw-Hill Comp.)
- [19] Abramowitz M and Stegun I A 1965 *Handbook of Mathematical Functions* (Dover Publ.)
- [20] Press W H *et al* 1992 *Numerical Recipes* (Cambridge: Cambridge University Press)
- [21] Pfeiffer C A, Economou E N and Ngai K L 1974 *Phys. Rev. B* **10**, 3038
- [22] Astratov V N *et al* 1999 *J. Light. Technol.* **17** 2050
- [23] Pendry J B and MacKinnon A 1992 *Phys. Rev. Lett.* **69** 2772
- [24] Markoš P and Soukoulis C M 2002 *Phys. Rev. E* **65** 036622